Radiofrequency Atomization and Excitation With a Hot Graphite Cup Electrode for Trace Element Determination by Atomic Emission Spectrometry

Kuniyuki Kitagawa and Takashi Katoh
Department of Applied Chemistry, School of Engineering, Nagoya University, Furo-cho, Chikusa-ku, Nagoya 464-01, Japan

A discharge lamp was constructed as an excitation source for the determination of trace elements in small samples by atomic emission spectrometry. A graphite cup, in which an aliquot (10 mg) of sample solution or powder was loaded, was located in a stainless-steel cylinder. An r.f. discharge was formed between the graphite cup and the grounded cylinder under a reduced pressure of argon. Concurrently with the formation of the plasma, the graphite cup was heated to about 1900 °C owing to the r.f. power dissipation. As a result, the sample was thermally vaporized and/or atomized, and subsequently excited to emit radiation in the discharge plasma surrounding the graphite cup. Basic characteristics were studied in conjunction with the analytical performance. The matrix effect of sodium was tested and found to be negligible in the determination of copper in the presence of up to a 1000-fold excess of sodium. A linear dynamic range of the calibration graph was obtained over about four orders of magnitude of analyte mass. The discharge lamp was applied to the direct determination of copper, zinc and chlorine in National Institute of Standards and Technology Standard Reference Materials of biological samples.

Keywords: *Atomic emission spectrometry; radiofrequency discharge lamp; hot cup electrode; atomization; small sample size*

As exemplified by the inductively coupled plasma (ICP), which has been widely used as a commercially available excitation source for trace element analysis, atomic emission spectrometry (AES) has advantageous features such as the capability for multi-element determinations and a wide dynamic range of analyte concentration.

Among the most recent requirements in analytical atomic spectrometry is the capability for multi-element determinations in small samples in a variety of matrices. In particular, this capability is important in clinical medicine, biochemistry, *etc.*, where large samples are rarely available. Electrothermal atomization atomic absorption spectrometry (ETAAS) is a well established technique that allows analyses of small samples.[1–3] However, multi-element AAS requires complex optical systems.

The development of a stable excitation source to permit multi-element determinations in small samples by analytical atomic spectrometry is important. Several techniques to satisfy these requirements have been developed for the ICP, *e.g.*, an electrothermal vaporizer,[4] direct insertion of a graphite sample cup[5,6] and a discrete nebulization technique where a small volume of sample solution was nebulized batchwise.[7]

In previous studies[8–10] several types of discharge lamps with a hot graphite cup electrode, which served as a sample vaporizer–atomizer, were developed. The atomized sample was subsequently excited in a plasma generated around the hot graphite cup. The use of radiofrequency (r.f.) power was found to be effective for high excitation of analyte atoms.

In this work, the basic characteristics of a newly constructed capacitively coupled r.f. discharge lamp were studied for trace analyses of small samples by AES. The r.f. discharge lamp was successfully applied to direct determinations of Cu, Zn and Cl in National Institute of Standards and Technology (NIST) Standard Reference Materials (SRMs) of biological samples.

Experimental

Radiofrequency Discharge Lamp and Instrumentation

Fig. 1 shows a schematic diagram of the capacitively coupled r.f. discharge lamp with a hot graphite cup electrode. The graphite cup of 3.5 mm i.d. and 5 mm o.d., 5 mm in height and 3.5 mm in depth (1), is fixed in a silicon carbide (SiC) cup of 5 mm i.d., 6 mm o.d. and 10 mm in height (2), which serves as a thermal resistor against the hot graphite cup. The SiC cup is attached to a molybdenum screw 3 mm in diameter and 53 mm in length (3). The SiC cup and the molybdenum screw are covered with an alumina tube of 6 mm i.d., 10 mm o.d. and 35 mm in length (4) (SSA-S, Nippon Kagaku Kogyo). The molybdenum screw is supported by a machinable glass ceramic (Macor) base (5), which serves as an electrical and thermal insulator. These components are incorporated in a cylindrical stainless-steel enclosure of 38 mm i.d., 60 mm o.d. and 77 mm in height (6), with quartz plate windows (7) for spectrometric observation (8). A quartz lid (9) serves as a window for

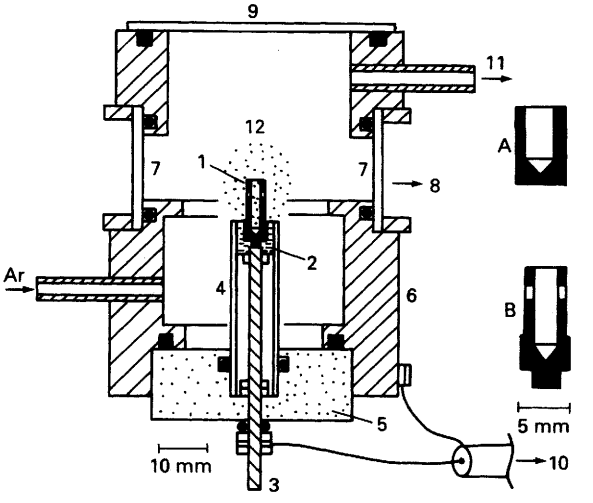

Fig. 1 Schematic diagram of the r.f. discharge lamp with a hot graphite cup electrode: 1, graphite cup; 2, SiC cup; 3, Mo screw; 4, alumina tube; 5, Macor base; 6, cylindrical stainless-steel enclosure (grounded); 7, quartz windows; 8, to spectrometer; 9, quartz lid; 10, to r.f. matching box; 11, to vacuum pump; and 12, r.f. plasma. A, graphite cup with plasma region (1–3 mm above cup) viewed laterally; and B, graphite cup with emission observed through aperture on lateral face

Table 1 Instrumentation

R.f. power supply system—	
Generator	Laboratory-made crystal oscillator
Power meter 1	Trio function power meter PF-810
Amplifier 1	Tokyo HyPower HL-400J
Power meter 2	Taniguchi Engineering Trades P2200
Amplifier 2	Tokyo HyPower HL-3K
Matching box	Daiwa Industry CNW-518
Dummy load	Kuranishi Keisoku Kenkyuusho RL-1200D
Spectrometer—	
Monochromator 1	Nippon Jarrell Ash JE-50E with a grating of 1200 grooves mm^{-1} and slits of 25 μm in width (spectral bandwidth = 0.04 nm)
Monochromator 2	Jobin Yvon H.20UV with a grating of 1200 grooves mm^{-1} and slits of 25 μm in width (spectral bandwidth = 0.1 nm)
Detector	Hamamatsu Photonics R666 photomultiplier tube (PMT)
PMT preamplifier	Laboratory made
PMT high-voltage supply	Laboratory made
Recording system—	
Recorder	Toa strip-chart recorder FBR-252A
Computer	NEC 9801UV11
A/D card	Designed by the Chubu Branch of the Japan Society for Analytical Chemistry
Program	Written in C-language (Turbo C Version 2.0)
Vacuum system—	
Vacuum meter	Okano Pirani gauge
Vacuum pump	Hitachi rotary pump C3A-150
Additional items—	
Optical pyrometer	Minolta TR-630
Microdispenser	Drummond Digital Microdispenser
Ar gas	Nihon Sanso (99.999%)

measuring the cup temperature by means of an optical pyrometer. At a flow rate of 50–240 ml min^{-1} STP, argon is forced to flow under a reduced pressure of 400–1866 Pa. The pressure was monitored with a Pirani gauge, whose sensor was attached to the vacuum line on the outlet side of the discharge lamp.

An r.f. power up to 400 W generated by an oscillator tuned at 13.56 MHz and two r.f. linear amplifiers was applied to the molybdenum screw through an impedance-matching circuit. As a result, a plasma discharge was formed between the graphite cup electrode and the grounded cylindrical enclosure (6). Thus, the graphite cup surrounded by the plasma was heated by the r.f. power dissipation. The time required for the graphite cup to reach an equilibrium temperature was 3–4 s. The r.f. power levels at the linear amplifiers were monitored by in-line transmission-type power meters. An alumina tube (4) prevented an undesirable discharge from being formed on the molybdenum screw surface and confined the effective discharge around the graphite cup.

Table 1 lists the components used for this study. Two spectrometers were used for the simultaneous detection of two analyte emissions or analyte and background emissions. The spectrometric signal acquired by a microcomputer through an analogue-to-digital (A/D) converter was processed to calculate the integrated emission after baseline correction.

Procedure for Measurement of Liquid Samples

An aliquot (10 μl) of a sample solution was placed in the graphite cup using a microdispenser (Drummond). Subsequently, pumping was started with the argon flow stopped. A reduced pressure of <133.3 Pa was reached when the solvent vaporization was considered to be completed. Then, the argon flow rate was adjusted to give a discharge pressure (400–1866 Pa at a flow rate of 50–240 ml min^{-1} STP). About 2 min later, the r.f. power was switched on for the sample atomization–excitation. The next run was made after cooling for about 3 min. Two types of graphite cup were used (Fig. 1, A and B). With type A, the plasma region from 1 to 3 mm above the top of the cup was viewed laterally by the spectrometer. With type B, the emission was observed through one of two apertures drilled on the lateral face of the graphite cup. The counter aperture prevents the black-body emission of the inner face from being viewed by the spectrometer. Type A was used throughout except for measuring the detection limits.

Procedure for Measurement of NIST Powder Samples

In order to attain stable excitation in the r.f. discharge plasma after the removal of biological matrices, electrothermal charring was applied to the NIST SRMs (SRM 1571 Orchard Leaves and SRM 1577 Bovine Liver). The same stainless-steel enclosure as that illustrated in Fig. 1 was used for the charring chamber. The discharge electrode was replaced with a cup-type graphite atomizer which served as a heating element for charring, or a charring cup.

An aliquot (0.15–2 mg) of the powdered sample was weighed into a graphite cup. For the standard additions method, 20 μl of a standard solution in 0.05 mol dm^{-3} sulfuric acid were added to the powdered sample. In order to prevent the powdered sample from being blown by a pressure shock on firing the discharge, the sample was covered with a graphite lid 3.2 mm in diameter and 1 mm in thickness; with the use of the lid, the emission peaks became broader but there was no decrease in the integrated emission, which was even slightly enhanced probably owing to the confinement of the resulting vapours. The graphite cup was then mounted in the charring cup. Under an argon purge, the sample was dried at about 100 °C for 1 min and then charred at 500 °C for 25 s by passing a current through the charring cup. Finally, the sample cup was transferred into the SiC cup of the discharge lamp and the discharge process described above was carried out.

Reagents

Stock standard solutions were prepared by dissolving metal sulfates or nitrates of analytical-reagent grade in distilled,

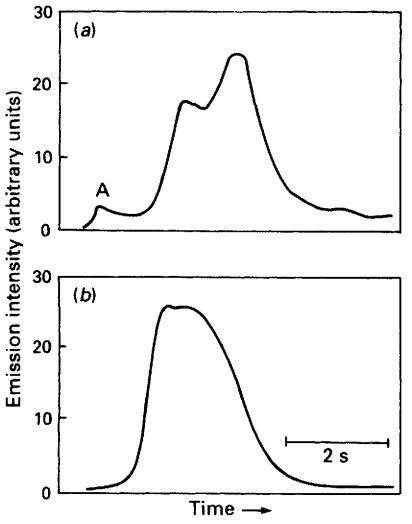

Fig. 2 Typical emission peaks for (*a*) Cu and (*b*) Na simultaneously measured by two separate spectrometers: A, peak of background emission (see text). The sample contains 10 ng of Cu (10 μl of 1 μg ml^{-1} $CuSO_4$) and Na (100 times the amount of Cu in moles) as Na_2SO_4. R.f. power, 300 W; Ar pressure, 10.664×10^2 Pa; λ_{Cu} = 324.75 nm and λ_{Na} = 589.99 nm

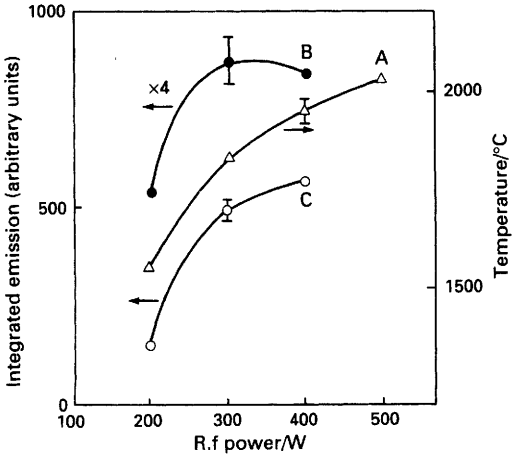

Fig. 3 Dependences of the graphite cup temperature and Cu emission intensity (integrated signal) on the r.f. power: A, temperature of cup; B, 100 ng of Cu (10 μl of 10 μg ml^{-1}); and C, 10 ng of Cu (10 μl of 1 μg ml^{-1}). Ar pressure, 7.198×10^2 Pa. For B, *y*-axis values should be multiplied by a factor of 4

de-ionized water and adjusting the acidity to 0.1 mol dm^{-3} with sulfuric acid or nitric acid of analytical-reagent grade. A stock chloride solution was prepared from magnesium chloride in the same manner. Argon of 99.999% purity and graphite of spectrometric grade were used throughout. Carbon tetrachloride vapour was mixed in the plasma gas for the wavelength setting of Cl. In order to enhance the emission intensity of Cl, 20% v/v helium in argon was used as the plasma gas.

Results and Discussion

Emission Peak Profile

A typical emission peak trace for copper is shown in Fig. 2. The first small peak (A) is the background emission, which was confirmed with a blank solution, displacing the spectrometer wavelength by about 0.1 nm from the 324.745 nm analytical line of Cu I. The most likely species responsible for the background emission are diatomic species such as

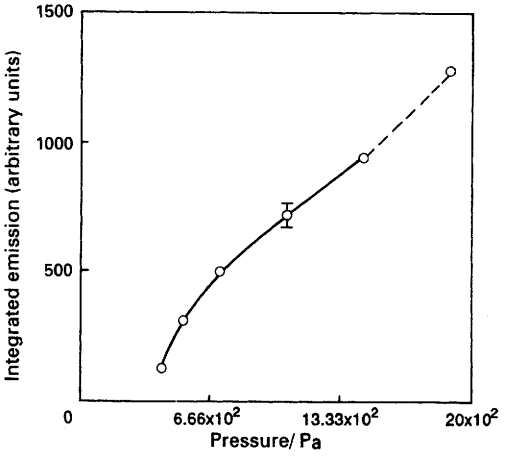

Fig. 4 Dependence of the Cu emission intensity (integrated signal) on the Ar pressure. The sample contains 10 ng of Cu; and r.f. power, 300 W

OH, N_2^+ and NH. The molecular emission from OH species (λ_{0-0} = 306.4 nm), N_2^+ (λ_{0-0} = 391.1 nm) and NH (λ_{0-0} = 335.8 nm) is known to be very strong in the 300–400 nm region. The species OH can be generated from the residual water of the sample solution. The species N_2^+, NH and NO can be evolved from the nitric acid.

The strong band of NO (λ_{0-0} = 226.2 nm) in the 200–300 nm region has been reported as a typical background source.[8,9] For the lines in a shorter wavelength region, Cd I 228.802 nm, Zn I 213.856 nm and Mg I 285.231 nm, however, the first peaks were found experimentally to be less intense than those for the lines in a longer wavelength region beyond 300 nm, Cu I 324.745 nm, Fe I 371.994 nm, Ag I 328.068 nm, Co I 346.580 nm, Cr I 357.869 nm, Al I 309.271 nm and V I 318.398 nm. Hence, the emissions from the species OH, N_2^+ and NH seem to be stronger than that from NO.

A high-speed scanning technique such as a refractor plate–a.c. amplifier combination and chemical modifiers would be effective in removing the background emission peaks.

Cup Temperature

Fig. 3 shows the dependence of the temperature of the graphite cup on the r.f. power. As the r.f. power increases, the cup temperature becomes higher but its increment decreases. The heat loss, through radiation according to the Stefan–Boltzmann law ($\propto T^4$), becomes larger at higher temperatures, resulting in the low increment of temperature. The integrated emission, for two different amounts of copper introduced, has an analogous dependence on the r.f. power to that of the cup temperature.

The temperature of the graphite cup determined by the r.f. power as described above was almost independent of the discharge pressure. On the other hand, the emission intensity (integrated signal) has a significant dependence on the pressure. As shown in Fig. 4, the integrated emission increases as the pressure becomes higher. Two possible causes are that the exciting species such as Ar*, Ar^+ and free electrons (which species is the most relevant is not clear) increase in number density and that the diffusion of the resulting atoms is confined or becomes slower at higher pressures. The former is likely because the emission peak profiles were broadened as the pressure became higher. At pressures >133.33 Pa, however, the discharge became unstable, forming a streamer which moved irregularly around the graphite cup.

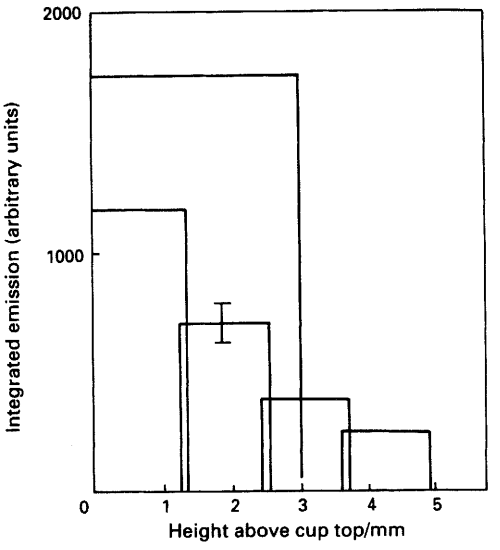

Fig. 5 Vertical distribution profile of the Cu emission intensity (integrated signal). The sample contains 100 ng of Cu; r.f. power, 400 W; and Ar pressure, 10.664×10^2 Pa. The width of the bar indicates the height of the vertical observation window, which is given by a horizontal slit located in front of the entrance slit of the spectrometer

Spatial Profile of Emission

The profile of the copper emission intensity (area) above the top of the type A graphite cup, which was obtained by moving the discharge lamp vertically is shown in Fig. 5. The emission intensity becomes lower at a higher position above the top of the graphite. This is mainly attributable to the decreased number density of atoms, caused by a rapid diffusion of the atomic vapour from the confined space in the cup to the free space around the cup. With the type B graphite cup, the emission from atoms at a higher number density is observable through the aperture. As a result, the detection limit [signal-to-noise ratio (S/N)=2] was about ten times lower (0.02 ng of copper) than that obtained with the type A graphite cup.

Calibration Graph and Detection Limit

The calibration graph for copper was linear from the detection limit up to 1×10^3 ng (about four orders of magnitude) and curved beyond 1×10^4 ng, whereas that of Cl was not linear. As shown in Fig. 6, however, the square of the integrated emission is proportional to the mass of Cl. This suggests that the dissociation of Cl_2 molecules plays a dominant role in the mechanisms involved: the equilibrium equation for Cl and Cl_2 explains the square dependence. In practice, green–yellowish radiation was visually observed around the graphite cup on firing the plasma. The radiation can probably be attributed to the molecular band of Cl_2, whose head lies at 516.3 nm.[11,12]

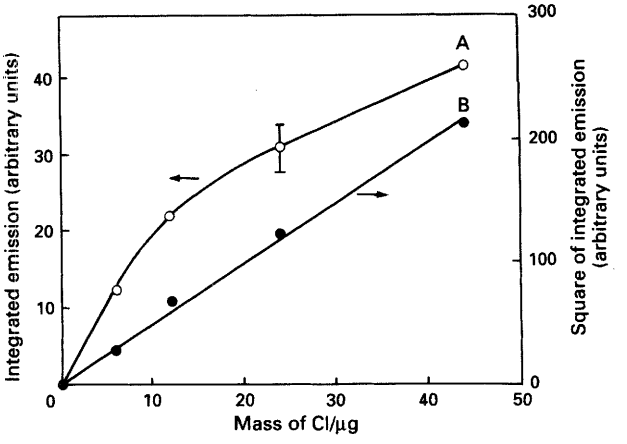

Fig. 6 Calibration graph for chlorine: A, integrated emission and B, square of integrated emission. Wavelength of Cl I, 460.10 nm; plasma gas, 20% v/v He in Ar; r.f. power, 300 W; and graphite cup temperature, 1600 °C. The sample contains $MgCl_2$

Detection limits obtained with the developed excitation source are listed in Table 2, together with those given by an ICP with an electrothermal vaporizer[4] and direct insertion of a graphite cup.[5,6] The detection limit obtained with the discharge lamp developed here is comparably low for copper compared with those attained by the other techiques, but higher for other elements. The use of helium or neon as the discharge gas possibly improves the detection limits through more effective excitation owing to its higher internal energy.

Effect of Easily Ionizable Elements

Another analytically important factor for an excitation source is freedom from matrix effects. An easily ionizable element (EIE), sodium, which is commonly present at

Table 2 Detection limts (DL)

		DL/ng*				DL/ng*	
Element	λ/nm	R.f. method	Ref.	Element	λ/nm	R.f. method	Ref.
Cu	324.75	0.02	0.02†	Cd	228.80	0.27	0.02† 0.03‡
Fe	371.99	0.12	0.04†	Ag	328.07	0.09	0.001‡
Mg	285.21	0.02		Mn	403.08	0.38§	0.02† 0.006‡
Zn	213.86	1.4§	0.02‡	Co	346.58	2.7	0.02†
Cr	357.87	1.2		Al	309.27	0.9	
Pb	405.78	3.8	0.035† 0.01‡	V	318.40	24	

*DL=detection limit based on $S/N=2$ ($S=s-b$ and $N=\sigma_b$, where s is the mean value of the peak height for the sample, b that for the blank and σ_b is the standard deviation of the peak heights for the blank). The type B graphite cup was used.

†From ref. 5.

‡From ref. 4.

§S is the peak height for the sample and N the baseline noise (range).

Table 3 Direct determinations of Zn, Cu and Cl in NIST SRMs

Sample	Element and line	Wavelength/nm	Found/$\mu g\ g^{-1}$* CM†	Found/$\mu g\ g^{-1}$* SAM‡	Certificate value/$\mu g\ g^{-1}$
SRM 1571 Orchard Leaves	Zn I	213.86	31 ± 5	26 ± 3	25 ± 3
SRM 1577 Bovine Liver	Cu I	324.75	179 ± 65	171 ± 55	193 ± 10
	Zn I	213.86	187 ± 40	129 ± 15	130 ± 10
	Cl I	460.10	3.3 ± 0.7§		2.6§,‖

*The standard deviation is based on the measurements repeated at least three times.
†CM = calibration method.
‡SAM = standard additions method.
§Values in mg g^{-1}.
‖Not certificate but reference value.

relatively high concentrations in most practical samples, was tested as a typical interferent as its coexistence often caused a notable enhancing effect on the analyte emission intensity in excitation sources such as a microwave-induced plasma[13] and a capacitively coupled microwave plasma[14] and in the reaction zone near the r.f. load coil of an ICP.[15] The dependence of the copper emission intensity (integrated signal) on the sodium concentration is shown in Fig. 7. The effect due to sodium is almost negligible up to a molar ratio of 1000 (mass of Na = 3622 ng). At a molar ratio of 10 000 (mass of Na = 36.22 μg), a suppressing effect is observed. This is mainly due to the plasma instability induced by the change in the discharge impedance, which is probably caused by the ionization of the large amount of sodium. Plasma fluctuation was visually observed and consequently induced impedance mismatching was indicated on the r.f. power meter. Use of an automatic impedance-matching circuit with a high response or a free-running r.f. generator could overcome the problem.

The reason why the effect due to sodium is small in the present discharge lamp is not completely clear. A possible cause is fractional vaporization which causes a separation of the residence time between copper and sodium atoms. Consequently, copper atoms emit under conditions free from sodium species. However, it was confirmed by experiment that this was not the case. In Fig. 2 the peak profile of sodium emission at 589.99 nm, which was simultaneously measured by another spectrometer, is shown, together with that of emission for copper. This illustrates that the copper and sodium atomic vapours co-existed during the majority of the residence time.

Another possible cause of the less significant EIE effect is as follows. Usually, the higher number density of free electrons in the plasma has been considered to play an important role in lessening the EIE effects in the analytical zone of the ICP.[16] As the number density of free electrons is not high under reduced pressure, it may not be a major factor responsible for the small effect due to sodium. However, spatial localization of free electrons due to a hollow effect, in which the electric field is condensed in the hollow graphite cup, resulting in a higher density of free electrons, might contribute to some extent to forming a high number density of free electrons around the graphite cup. Experimental observation of the number density of free electrons, using the Hβ line,[17] requires detailed discussion.

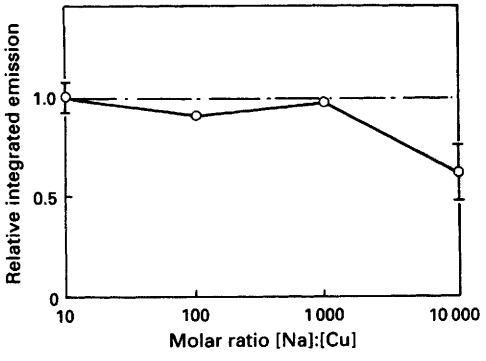

Fig. 7 Dependence of the Cu emission intensity (integrated signal) on the co-existing concentration of Na: mass of Cu, 10 ng; r.f. power, 300 W; and Ar pressure, 7.198×10^2 Pa. The abscissa is the relative integrated emission with respect to the integrated emission in the absence of Na

Application to NIST Biological Standard Reference Materials

The optimization of charring is important in the direct determination of trace elements in solid or powder samples without applying chemical digestion. In a preliminary experiment, charring of the NIST powder samples was effected in a pre-discharge which was obtained at an r.f. power lower than 100 W, before the main discharge for atomization–excitation. However, intensive atomic emission was observed in the pre-discharge process, which implies analyte loss. This is probably attributable to plasma sputtering. A conventional charring method used in ETAAS was therefore employed, as described under Experimental.

The discharge was occasionally unstable after charring at temperatures lower than 400 °C, whereas the loss of copper and zinc was found after charring above 600 °C. Accordingly, 500 °C was chosen as the optimum charring temperature. After applying optimized charring, the peak profiles of copper, zinc and chlorine emissions observed with the NIST sample were almost the same as those obtained with the standard solutions.

The results for the NIST SRMs are given in Table 3. Fairly good agreement between the values obtained with the standard additions method and those certified by NIST, with relative errors within 11%, was obtained for copper and zinc. Positive errors were found in the zinc determinations with the calibration method, which reflects some chemical interferences. The relative error of 27% for chlorine is much larger than that for copper or zinc. In practice, the blank signal was much higher (about ten times) in magnitude and fluctuated more than those for other elements. Insufficient purification of water or some background-emitting species might be responsible.

Conclusions

An r.f. discharge lamp with a hot graphite cup electrode was constructed for trace element analyses of small samples by AES. Its basic characteristics and analytical performance were examined. The atomization seems to be principally

thermal (see the high detection limit for vanadium). As seen from the aluminium loss in the pre-discharge, described above, however, sputtering caused by the plasma species such as Ar^+ can also play a role. A wide linear dynamic range of about four orders of magnitude of concentration was obtained. The EIE effect caused by an excess amount of co-existing sodium was negligibly small up to an [Na]:[Cu] relative molar ratio of 1000. Application to the trace determination of copper, zinc and chlorine in NIST Standard Reference Materials was made with fairly good agreement with the certificate values.

The authors thank S. Takahashi for manufacturing the discharge tube and T. Watanabe and T. Imura for fine processing of the ceramic tubes. This research was partly supported by a Grant-in-Aid from the Ministry of Education, Science and Culture, Japan.

References

1 Wennrich, R., Bonitz, U., Brauer, H., Niebegall, K., and Dittrich, K., *Talanta*, 1985, **32**, 1035.
2 Chakrabarti, C. L., Delgado, A. H., Chang, S. B., Falk, H., Hutton, T. J., Runde, G., Sychra, V., and Dolezal, J., *Spectrochim. Acta, Part B*, 1986, **41**, 1075.
3 Itoh, K., and Atsuya, I., *Bunseki Kagaku*, 1986, **35**, 530.
4 Gunn, A. M., Millard, D. L., and Kirkbright, G. F., *Analyst*, 1978, **103**, 1066.
5 Kirkbright, G. F., and Walton, S. J., *Analyst*, 1982, **107**, 276.
6 Abdullah, M., Fuwa, K., and Haraguchi, H., *Appl. Spectrosc.*, 1987, **41**, 715.
7 Uchida, T., Kojima, I., Iida, C., and Goto, K., *Analyst*, 1986, **111**, 791.
8 Kitagawa, K., Narita, R., and Takeuchi, T., *Anal. Chim. Acta*, 1979, **110**, 291.
9 Kitagawa, K., Kanoh, S., Ohta, K., and Yanagisawa, M., *Anal. Sci.*, 1988, **4**, 153.
10 Kitagawa, K., Katoh, S., and Yanagisawa, M., *J. Spectrosc. Soc. Jpn.*, 1989, **38**, 209.
11 Huber, K. P., and Herzberg, G., *Diatomic Molecules and Spectra*, Van Nostrand Reinhold, New York, 1979.
12 Clyne, M. A. A., and Coxon, J. A., *Proc. R. Soc. London, Ser. A*, 1967, **298**, 424.
13 Matousek, J. P., Orr, B. J., and Selby, M., *Spectrochim. Acta, Part B*, 1986, **41**, 415.
14 Kitagawa, K., Koyama, T., and Takeuchi, T., *Anal. Chim. Acta*, 1979, **109**, 241.
15 Kawaguchi, H., Ito, T., Ohta, K., and Mizuike, A., *Spectrochim. Acta, Part B*, 1980, **35**, 204.
16 Haraguchi, H., *ICP Hakkobunseki no Kiso to Ouyou*, Koudansha, Tokyo, 1986.
17 Blades, M. W., and Caughlin, B. L., *Spectrochim. Acta, Part B*, 1985, **40**, 579.

Paper 1/04457E
Received August 27, 1991
Accepted November 26, 1991